

Supporting information on:

Weak hydrogen bonding to halogens and chirality communication in propanols: Raman and microwave spectroscopy benchmarks theory

Beppe Hartwig^a, Melanie Schnell^{b,c}, Martin A. Suhm^a and Daniel A. Obenchain*^a

a Institut für Physikalische Chemie, Georg-August-Universität Göttingen, Tammannstr. 6, 37077 Göttingen, Germany. E-mail: daniel.obenchain@uni-goettingen.de

b Deutsches Elektronen-Synchrotron DESY, Notkestr. 85, Hamburg, Germany.

c Institute of Physical Chemistry, Christian-Albrechts-Universität zu Kiel, Max-Eyth-Straße 1, Kiel, Germany.

Contents

1 Experimental parameters	1
2 Energetics	2
3 Vibrational data	5
4 Rotational data	7
5 Conversion of τ to the quartic centrifugal distortion constants	12
6 Additional vibrational analysis	13
7 Example inputs	16
7.1 ORCA	16
7.2 Gaussian	17
7.3 Molpro	17
Literature	18

Large parts of the content provided here have previously been published in Ref. [1]. Additionally, Experimental details as well as the raw vibrational spectra (DOI:10.25625/EJVBHD), relative electronic and zero point corrected energies, vibrational assignments, predicted/experimental rotational constants, rotational line lists, CCSD(T) xyz-files, are published as a separate dataset. Raw cavity microwave data is provided in a separate dataset.

1 Experimental parameters

In the following, T_S is the saturator temperature, T_N the nozzle temperature, d_N the distance of the laser from the nozzle, N the number of averaged exposures, t_{exp} the length of each exposure, p_S the stagnation pressure and ν the frequency range if applicable. Cavity transitions were measured on the Q-CUMBER FTMW spectrometer in Göttingen,^[2] using the FTMW++ program of Grabow.^[3] Cavity data is made available on the GRO.data archive. CITE GRO.DATA

Tab. S1: Overview of the experimental conditions for the Raman spectra discussed in the main text. The raw spectra have been made available in Ref. [4] and have been plotted in Fig. S3. All spectra have been recorded in pure He.

compound	T_S / K	T_N / K	d_N / mm	$N \times t_{\text{exp}}$ / min	p_S / bar
1-chloropropan-2-ol	275	300	1.0	24×4	0.4
2-chloropropan-1-ol	275	300	1.0	18×4	0.4
1-bromopropan-2-ol	285	300	1.0	10×4	0.6
2-bromopropan-1-ol	285	300	1.0	8×4	0.6

Tab. S2: Overview of the experimental conditions for the microwave spectra discussed in the main text. For the microwave setups the nozzle acts as the saturator. Hence, only T_N is given. Here, N refers to the amount of averaged free induction decays (FIDs). The bromopropanol parameters given correspond to the COMPACT setup. For the QCUMBER setup, individual transitions are measured and N varies greatly depending upon the intensity of the transition. Therefore, a general upper and lower bound is given instead. All spectra have been recorded in pure Ne.

compound	ν / GHz	T_N / K	$N / 10^3$	p_S / bar
1-bromopropan-2-ol	2 – 8	325	4700	2.4
2-bromopropan-1-ol	2 – 8	300	4300	2.4
QCUMBER	6 – 18	300	0.1 – 10	1.4

Tab. S3: Overview of the used chemicals. CAS-numbers, suppliers, purity and the setups where they have been measured are also given. 70% purity indicates technical grade, with the largest impurity being 2-bromopropan-1-ol for 1-bromopropan-2-ol and 2-chloropropan-1-ol for 1-chloropropan-2-ol.

compound	CAS-number	supplier	purity	setup
1-bromopropan-2-ol	19686-73-8	Sigma-Aldrich	70%	curry, COMPACT, QCUMBER
2-bromopropan-1-ol	598-18-5	BLD	97%	curry, COMPACT
1-chloropropan-2-ol	127-00-4	TCI	70%	curry, QCUMBER
(R)-1-chloropropan-2-ol	19141-39-0	BLD	98%	curry
(R)-2-chloropropan-1-ol	37493-14-4	BLD	95%+	curry

He	7440-59-7	Nippon Gas	99.996%	<i>curry</i>
Ne	7440-01-9	Linde Gas	99.9990%	COMPACT, QCUMBER

2 Energetics

Tab. S4: Comparison of energetical computational data with literature values from Gonçalves *et al.*^[5] for 1-bromopropan-2-ol and 2-bromopropan-1-ol. The relative electronic energy (ΔE_{el}) and harmonically zero point corrected energy (ΔE_0^{h}) as well as the anharmonically corrected energies (ΔE_0^{an}), if available, are shown. In case of the literature data it is not entirely clear if zero point correction was applied. The energies are given relative to the most stable (gG') conformer. The VDZ-F12* basis set is defined as all = VDZ-F12 and Br = VDZ-PP-F12. All values are given in kJ mol⁻¹.

	2-bromopropan-1-ol			1-bromopropan-2-ol		
	ΔE_{el}	ΔE_0^{h}	ΔE_0^{an}	ΔE_{el}	ΔE_0^{h}	ΔE_0^{an}
BP86/maTZ	1.46	1.79	-	1.27	1.25	-
PBE/maTZ	1.76	2.07	-	2.29	2.22	-
PBE0/maTZ	1.61	1.94	-	2.20	2.18	-
B3LYP/maTZ	1.45	1.73	-	2.19	2.17	-
TPSS/aVTZ	1.34	1.61	1.59	1.96	1.96	1.94
PBE0/aVTZ	1.76	2.06	2.10	2.33	2.29	2.16
B3LYP/aVTZ	1.55	1.80	1.79	2.23	2.20	1.94
CAM-B3LYP/aVTZ	1.65	1.90	1.92	3.02	3.00	2.95
B2PLYP/aVTZ	1.64	1.92	1.98	2.73	2.70	2.65
MP2/aVTZ	1.22	1.50	1.50	2.43	2.39	2.20
CCSD(T)-F12a/VDZ-F12*	0.43	0.78	-	2.44	2.36	-
B3LYP/aug-cc-pVDZ ^[5]	-	-	-	4.10	-	-
MP2/6-311++G(d,p) ^[5]	-	-	-	4.02	-	-

Tab. S5: Comparison of energetical computational data with literature values from Goldstein *et al.*^[6] and Gonçalves *et al.*^[5] for 1-chloropropan-2-ol and 2-chloropropan-1-ol. The relative electronic energy (ΔE_{el}) and harmonically zero point corrected energy (ΔE_0^{h}) as well as the anharmonically corrected energies (ΔE_0^{an}) if available are shown. In case of the literature data it is not entirely clear if zero point correction was applied. The energies are given relative to the most stable (gG') conformer. All values are given in kJ mol⁻¹.

	2-chloropropan-1-ol			1-chloropropan-2-ol		
	ΔE_{el}	ΔE_0^{h}	ΔE_0^{an}	ΔE_{el}	ΔE_0^{h}	ΔE_0^{an}
BP86/maTZ	1.62	1.92	-	1.93	1.94	-
PBE/maTZ	1.91	2.20	-	2.71	2.70	-
PBE0/maTZ	1.75	2.07	-	2.61	2.63	-
B3LYP/maTZ	1.62	1.89	-	2.59	2.60	-
TPSS/aVTZ	1.50	1.74	1.87	2.41	2.46	2.54
PBE0/aVTZ	1.90	2.18	2.27	2.76	2.78	2.64
B3LYP/aVTZ	1.72	1.95	1.75	2.66	2.67	2.46
CAM-B3LYP/aVTZ	1.83	2.06	2.09	3.32	3.33	3.26
B2PLYP/aVTZ	1.87	2.10	2.44	3.67	3.70	3.56
MP2/aVTZ	1.47	1.69	1.68	3.14	3.20	3.20

CCSD(T)-F12a/VDZ-F12	1.36	1.59	-	3.22	3.26	-
B3LYP/aug-cc-pVDZ ^[5]	-	-	-	4.14	-	-
MP2/6-311++G(d,p) ^[6]	0.78	-	-	3.93	-	-
MP2/6-311++G(d,p) ^[5]	-	-	-	3.93	-	-

Tab. S6: Relative energies between primary (2-X-propan-1-ol) and secondary (1-X-propan-2-ol) alcohol configuration are shown, with X being Cl and Br. The relative electronic energy (ΔE_{el}) and harmonically zero point corrected energy (ΔE_0^{h}) as well as the anharmonically corrected energies (ΔE_0^{an}) if available are shown. Energy differences are taken from the respective most stable conformers. All values are given in kJ mol^{-1} .

	chloropropanol			bromopropanol		
	ΔE_{el}	ΔE_0^{h}	ΔE_0^{an}	ΔE_{el}	ΔE_0^{h}	ΔE_0^{an}
BP86/maTZ	1.37	1.65	-	1.76	2.09	-
PBE/maTZ	2.13	2.40	-	2.88	3.19	-
PBE0/maTZ	2.48	2.82	-	3.40	3.80	-
B3LYP/maTZ	2.12	2.47	-	2.97	3.39	-
TPSS/aVTZ	1.65	2.02	1.91	2.56	3.00	2.89
PBE0/aVTZ	2.41	2.75	2.61	3.49	3.91	3.83
B3LYP/aVTZ	2.02	2.37	2.21	3.02	3.46	3.44
CAM-B3LYP/aVTZ	3.34	3.71	3.64	4.84	5.31	5.30
B2PLYP/aVTZ	3.11	3.53	3.10	3.24	3.77	3.65
MP2/aVTZ	2.32	2.80	2.75	1.96	2.54	2.39
CCSD(T)-F12a/VDZ-F12*	3.27	3.74	-	6.38	6.59	-

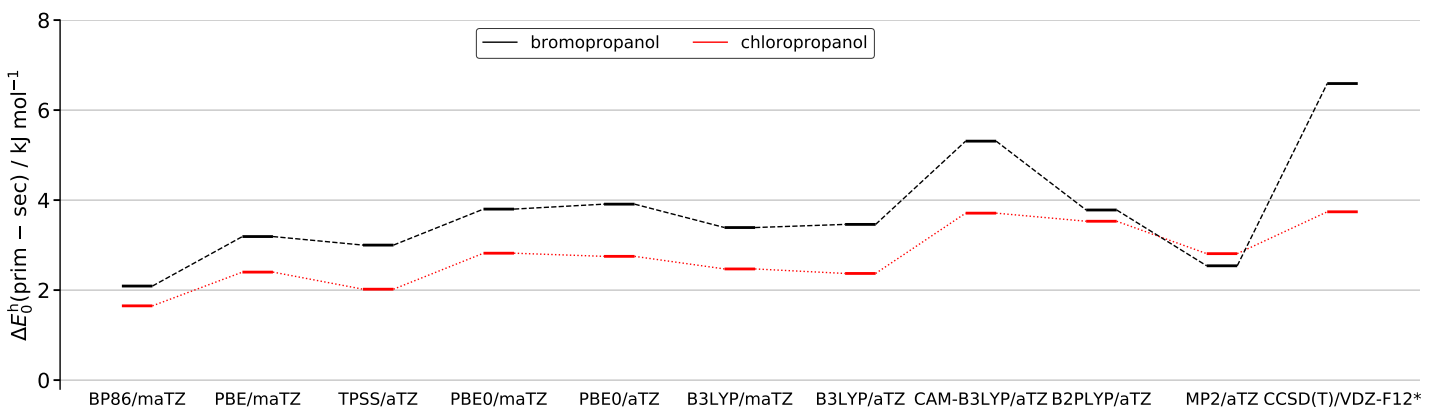


Fig. S1: Relative harmonic zero point corrected energies between the primary (2-X-propan-1-ol) and secondary (1-X-propan-2-ol) alcohol configuration are shown for the bromopropanols (black) and chloropropanols (red). In all cases the secondary alcohol is energetically favoured. With the exception of MP2, all methods predict the secondary alcohol to be even more favoured for the bromopropanols. Furthermore, CAM-B3LYP best reproduces the trend indicated by the coupled cluster calculations. Energy differences are taken from the respective most stable conformers. The raw data can be found in Tab. S6.

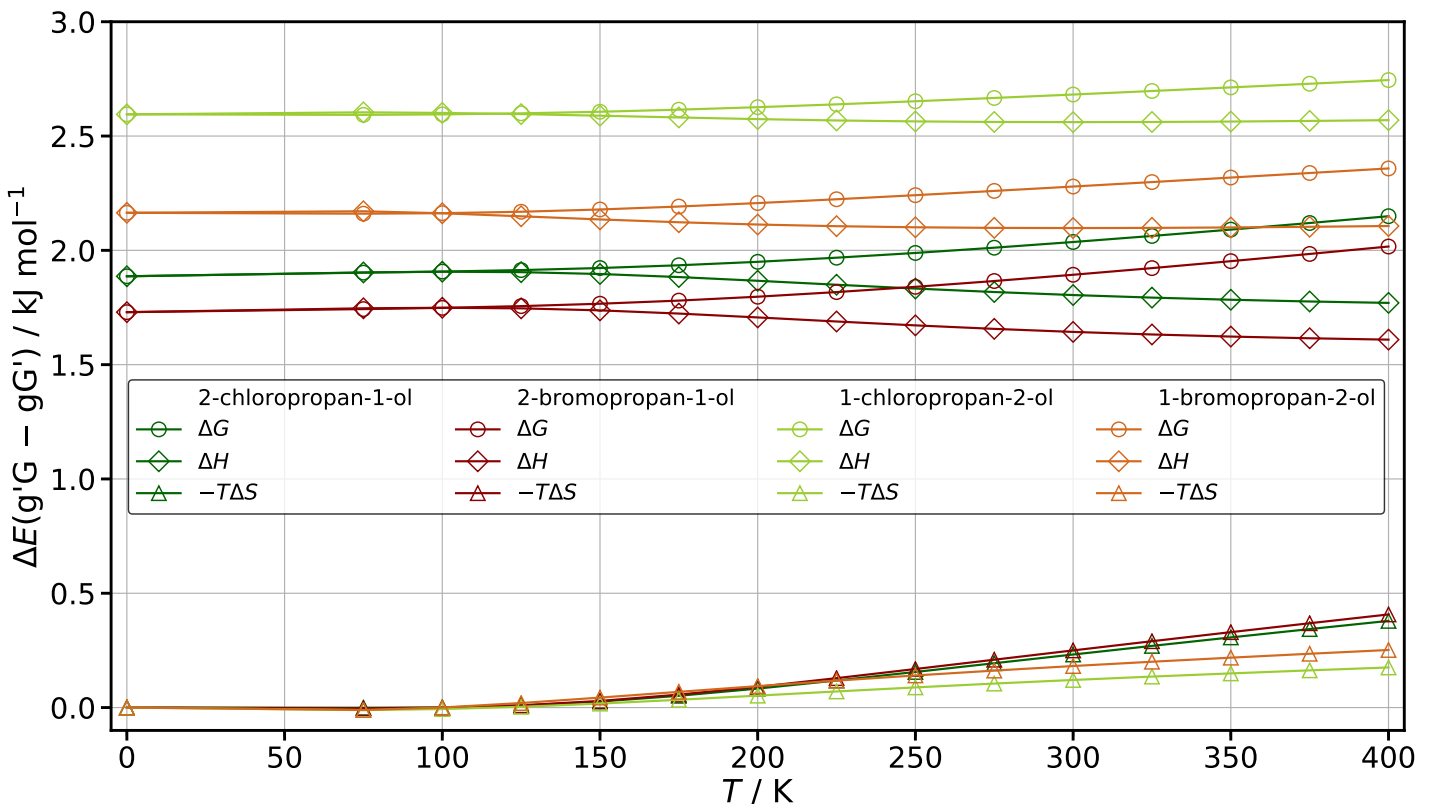


Fig. S2: Temperature dependent behaviour of the relative free Gibbs energy (ΔG), relative enthalpy (ΔH) and relative negative product of the temperature and entropy ($-T\Delta S$) for 2-chloropropan-1-ol (dark green), 2-bromopropan-1-ol (brown), 1-chloropropan-2-ol (light green), and 1-bromopropan-2-ol (orange). The, in all cases, more stable gG' conformer is used as a reference point. The calculations were conducted with ORCA (version 4.2.1) using the B3LYP-D3(BJ,abc)/ma-def2-TZVP method and default settings for the computation of thermodynamic properties which includes the Quasi Rigid Rotor Harmonic Oscillator approximation of S. Grimme^[7]. For ΔG , a continuous slight increase in the energy difference between g'G and gG' can be observed, *i.e.* an increased chiral induction effect. However, the change is rather small with at most +0.29 kJ mol⁻¹ in case of 2-bromopropan-1-ol. This is due to the fact that ΔH and $-T\Delta S$ partially compensate each other with the entropy contribution leading to a slight energetic favourability of the gG' conformer. Furthermore, the the bromine analogues have slightly larger entropy contributions than the chlorine ones. We expect the general trends observed for B3LYP-D3(BJ,abc)/ma-def2-TZVP to also hold true for more sophisticated methods such as B2PLYP or coupled cluster.

3 Vibrational data

Tab. S7: Overview of the predicted and measured OH stretching frequencies of the bromopropanols. The prefix 2- refers to the corresponding 2-bromopropan-1-ol conformers and 1- to the 1-bromopropan-2-ol ones. $\tilde{\nu}^h$ and $\tilde{\nu}^{an}$ refer to harmonic and anharmonic values, respectively. The VDZ-F12* basis set is defined as all = VDZ-F12 and Br = VDZ-PP-F12. In the nomenclature of Goldstein *et al.*[6], g-ga, g'-gg, m-ga and h-gg correspond to 2-gG', 2-g'G, 1-gG' and 1-g'G, respectively. All values are given in cm^{-1} .

	2-gG'		2-g'G		1-gG'		1-g'G	
	$\tilde{\nu}^h$	$\tilde{\nu}^{an}$	$\tilde{\nu}^h$	$\tilde{\nu}^{an}$	$\tilde{\nu}^h$	$\tilde{\nu}^{an}$	$\tilde{\nu}^h$	$\tilde{\nu}^{an}$
Raman-Jet	-	3607	-	3608	-	3608	-	3598
BP86/mTZ	3601.04	-	3607.85	-	3606.05	-	3604.68	-
PBE/mTZ	3611.71	-	3618.68	-	3615.94	-	3614.72	-
TPSS/aTZ	3629.49	3430.55	3633.93	3436.63	3631.04	3436.75	3628.68	3432.99
PBE0/mTZ	3801.03	-	3805.63	-	3804.33	-	3799.87	-
PBE0/aTZ	3805.79	3617.99	3810.12	3621.99	3809.09	3625.22	3803.77	3616.82
B3LYP/mTZ	3749.72	-	3753.52	-	3753.86	-	3748.00	-
B3LYP/aTZ	3762.88	3573.32	3766.75	3578.38	3766.58	3581.12	3760.43	3571.55
CAM-B3LYP/aTZ	3812.09	3632.72	3815.15	3636.97	3815.20	3639.09	3806.91	3629.12
B2PLYP/aTZ	3779.12	3592.11	3783.35	3596.97	3777.72	3593.68	3772.35	3585.97
MP2/aTZ	3775.57	3590.69	3775.83	3591.35	3766.79	3583.87	3764.61	3580.81
CCSD(T)-F12a/VDZ-F12*	3794.68	-	3794.98	-	3790.80	-	3783.96	-

Tab. S8: Overview of the predicted and measured OH stretching frequencies of the chloropropanols. The prefix 2- refers to the corresponding 2-chloropropan-1-ol conformers and 1- to the 1-chloropropan-2-ol ones. $\tilde{\nu}^h$ and $\tilde{\nu}^{an}$ refer to harmonic and anharmonic values, respectively. The MP2/6-311++G(d,p) results of Goldstein *et al.*[6] were originally scaled by 0.95. In the nomenclature of Goldstein *et al.*[6], g-ga, g'-gg, m-ga and h-gg correspond to 2-gG', 2-g'G, 1-gG' and 1-g'G, respectively. All values are given in cm^{-1} .

	2-gG'		2-g'G		1-gG'		1-g'G	
	$\tilde{\nu}^h$	$\tilde{\nu}^{an}$	$\tilde{\nu}^h$	$\tilde{\nu}^{an}$	$\tilde{\nu}^h$	$\tilde{\nu}^{an}$	$\tilde{\nu}^h$	$\tilde{\nu}^{an}$
Jet	-	3620	-	3620	-	3619	-	3609
BP86/maTZ	3621.07	-	3626.90	-	3623.18	-	3622.14	-
PBE/maTZ	3632.35	-	3638.32	-	3633.76	-	3633.01	-
TPSS/aVTZ	3649.71	3455.43	3653.45	3458.37	3648.99	3457.46	3646.84	3453.96
PBE0/maTZ	3816.01	-	3819.92	-	3817.46	-	3813.04	-
PBE0/aVTZ	3821.13	3635.89	3824.49	3640.49	3822.24	3641.52	3816.91	3633.68
B3LYP/maTZ	3761.07	-	3764.53	-	3763.39	-	3757.88	-
B3LYP/aVTZ	3775.00	3587.81	3777.97	3592.13	3776.70	3593.12	3770.54	3584.26
CAM-B3LYP/aVTZ	3820.74	3642.89	3823.19	3645.58	3822.25	3647.49	3814.25	3637.56
B2PLYP/aVTZ	3791.56	3606.23	3793.37	3609.14	3788.70	3606.33	3783.15	3598.85
MP2/6-311++G(d,p) ^[6]	3862.11	-	3864.21	-	3852.63	-	3852.63	-
MP2/aVTZ	3792.61	3611.03	3793.08	3611.62	3783.05	3603.04	3780.37	3599.60
CCSD(T)-F12a/VDZ-F12	3808.94	-	3808.68	-	3805.09	-	3797.65	-

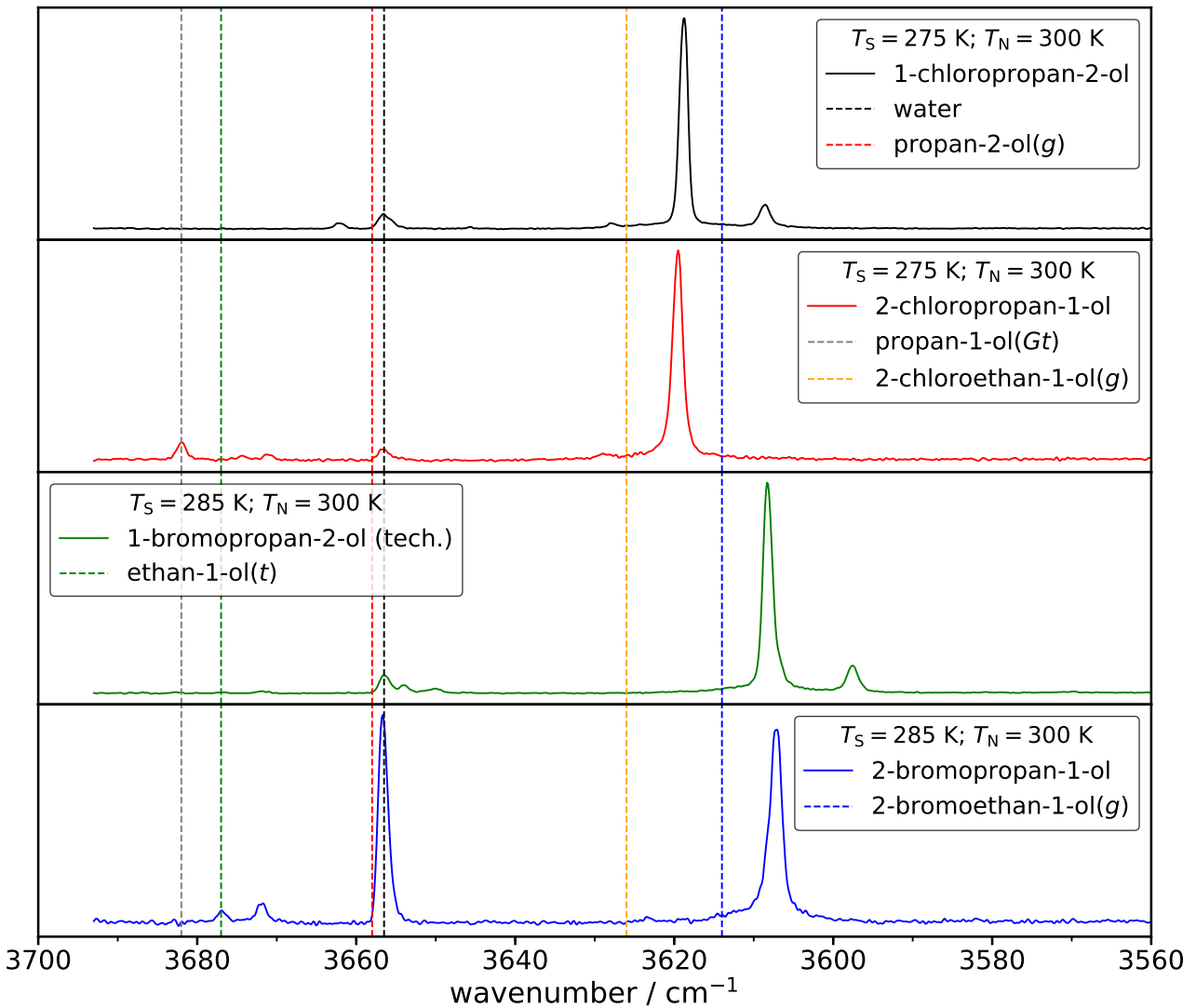


Fig. S3: Overview of the Raman spectra for 1-chloropropan-2-ol (black trace), 2-chloropropan-1-ol (red trace), 1-bromopropan-2-ol (green trace) and 2-bromopropan-1-ol (blue trace) as published in Ref. [4]. Details with regards to the purity and experimental conditions can be found in Tabs. S3 and S1, respectively. The saturator (T_S) and nozzle temperatures (T_N) are given. The dashed lines indicate the band positions (jet values with the exception of 2-bromoethan-1-ol) of a variety of possible impurities. The following bands are shown: water (3657 cm^{-1})^[8] ethan-1-ol (*trans*: 3677 cm^{-1} , *gauche*: 3659 cm^{-1})^[9], propan-1-ol (*Gt*: 3682 cm^{-1})^[10], propan-2-ol (*gauche*: 3658 cm^{-1})^[11], 2-chloroethan-1-ol (*gauche*: 3626 cm^{-1})^[12] and 2-bromoethan-1-ol (*gauche*: 3614 cm^{-1})^[13]. Some of the listed values that were obtained with Raman spectroscopy have been corrected with regards to a calibration error. The values shown are for the most stable conformer which are populated the strongest under jet conditions. Hence, if the corresponding most stable conformer cannot be observed the compound is either not present or only in insignificant amounts. Trace amounts of water are always present in the jet and fluctuate between different measurements. The spectrum of 2-bromopropan-1-ol was recorded before changes to the Raman setup were made which greatly reduced the water content as can be seen from the other later measurements. In case of 2-chloropropan-1-ol, minor impurities of propan-1-ol may be present with only the most stable *Gt* conformer being indicated (others not shown). For 2-bromopropan-1-ol, minor amounts of the *trans* conformer of ethan-1-ol may be present. No evidence for the *gauche* conformer can be found. For the other impurities that are deemed likely, no matching bands can be observed. It might be the case, that some of the bands can be attributed to fluorescence of the compound itself or other impurities within it. However, time-dependent DFT calculations (without the Tamm-Dancoff-Approximation), using CAM-B3LYP-D3(BJ,abc)/ma-def2-TZVP a functional, for the choloro- and bromopropanols suggest that no electronic transitions are accessible by a 532 nm laser. The closest transitions lie around 170 nm and 200 nm for the chloro- and bromopropanols, respectively. Decomposition products may also play a role. Note that the original Raman spectra cover a range from 3700 cm^{-1} to 3250 cm^{-1} with no additional signals arising in the lower wavenumber range.

4 Rotational data

Tab. S9: Overview of the experimentally determined rotational constants for 2-bromopropan-1-ol (top) and 1-bromopropan-2-ol (bottom) for the two naturally abundant bromine isotopes. All other isotopes are in their most naturally abundant form. The Watson S Hamiltonian was used for all fits. Furthermore, the microwave root mean squared deviation σ_{RMS} and the number of assigned lines N_L are given as well as the maximum value of the (pseudo)-quantum numbers J^m , K_a^m , K_c^m and F^m involved in the assigned transitions and Ray's asymmetry parameter κ ^[14]. Moreover, it is noted whether or not transitions according to μ_a , μ_b or μ_c dipole components were observed. All values are given in MHz when applicable. Values in brackets for χ_{ij} were computed at the CCSD(T)-DKH2/awCVTZ level of theory and were fixed during the fit. In the nomenclature of Goldstein *et al.*^[6], g-ga, g'-gg, m-ga and h-gg correspond to 2-gG', 2-g'G, 1-gG' and 1-g'G, respectively.

	2-gG'		2-g'G	
	⁷⁹ Br	⁸¹ Br	⁷⁹ Br	⁸¹ Br
<i>A</i>	3948.083 05(45)	3944.438 22(52)	4677.437 40(70)	4675.665 73(66)
<i>B</i>	2349.194 09(32)	2328.608 08(31)	2079.364 10(29)	2061.302 89(26)
<i>C</i>	1553.406 49(23)	1543.825 73(22)	1675.648 75(26)	1663.689 85(24)
D_J	0.000 728 9(98)	0.000 719 2(92)	0.000 657 8(80)	0.000 659 3(83)
D_K	0.001 657(33)	0.001 653(36)	0.004 303(80)	0.004 595(90)
D_{JK}	-0.000 872(13)	-0.000 795(17)	-0.000 932(17)	-0.000 934(15)
d_1	-0.000 310 9(39)	-0.000 296 0(25)	-0.000 194 1(23)	-0.000 188 9(20)
d_2	-0.000 044 5(14)	-0.000 045 2(10)	-0.000 021 51(90)	-0.000 016 95(91)
χ_{aa}	304.3578(20)	257.0380(24)	317.5501(27)	266.3215(23)
χ_{bb-cc}	144.5718(38)	118.1296(44)	68.1424(48)	56.1224(44)
χ_{ab}	304.968(83)	253.085(78)	266.30(10)	221.81(11)
χ_{ac}	144.41(25)	120.58(22)	-199.72(17)	-166.71(19)
χ_{bc}	87.55(18)	72.68(10)	-103.801(65)	-86.347(72)
C_{aa}	0.003 28(29)	0.003 74(38)	0.003 72(45)	0.003 10(39)
C_{bb}	0.003 62(19)	0.003 68(23)	0.002 84(25)	0.002 71(20)
C_{cc}	0.002 38(20)	0.002 82(25)	0.002 49(26)	0.002 80(24)
μ_a	yes	yes	yes	yes
μ_b	yes	yes	yes	yes
μ_c	yes	yes	yes	yes
σ_{RMS}	0.0037	0.0048	0.0054	0.0046
N_L	176	185	233	229
$J^m/K_a^m/K_c^m/F^m$	6/4/5/7.5	9/4/9/7.5	9/3/7/9.5	8/3/7/9.5
κ	-0.34	-0.35	-0.73	-0.74
	1-gG'		1-g'G	
	⁷⁹ Br	⁸¹ Br	⁷⁹ Br	⁸¹ Br
<i>A</i>	8428.619 77(93)	8428.402 12(95)	5881.083 84(15)	5879.489 28(21)
<i>B</i>	1438.940 45(15)	1426.181 64(17)	1710.470 287(40)	1695.948 564(62)
<i>C</i>	1284.319 36(17)	1274.149 41(17)	1608.464 009(41)	1595.727 914(58)
D_J	0.000 191 0(28)	0.000 187 3(23)	0.000 447 88(70)	0.000 445 4(13)
D_K	0.005 88(12)	0.005 90(16)	-0.000 535(37)	-0.000 553(54)
D_{JK}	0.002 097(34)	0.002 078(30)	0.002 367 0(43)	0.002 351 2(65)
d_1	-0.000 021 98(60)	-0.000 023 76(68)	-0.000 010 05(33)	-0.000 010 35(49)
d_2	-	-	-0.000 001 35(17)	-0.000 001 81(31)

χ_{aa}	367.4395(28)	306.9980(31)	222.965 00(87)	186.9387(10)
χ_{bb-cc}	126.1196(48)	105.4264(52)	-338.5308(14)	-282.1467(18)
χ_{ab}	291.540(25)	243.619(31)	-13.775(95)	-12.44(25)
χ_{ac}	-138.418(68)	-115.310(85)	-386.9640(46)	-323.096(10)
χ_{bc}	-72.930(29)	-60.875(37)	[-1.438]	[-1.216]
C_{aa}	0.002 66(81)	0.001 05(93)	0.003 41(14)	0.003 42(21)
C_{bb}	0.001 75(21)	0.001 53(23)	0.002 118(68)	0.002 22(10)
C_{cc}	0.001 43(20)	0.001 12(21)	0.001 107(61)	0.001 188(86)
μ_a	yes	yes	yes	yes
μ_b	yes	yes	yes	yes
μ_c	yes	yes	yes	yes
σ_{RMS}	0.0046	0.0052	0.0040	0.0042
N_L	193	196	295	290
$J^m/K_a^m/K_c^m/F^m$	9/3/8/9.5	9/3/9/10.5	10/2/10/11.5	10/3/10/11.5
κ	-0.96	-0.96	-0.95	-0.95

Tab. S10: Overview of the experimentally determined rotational constants for 2-chloropropan-1-ol (top) and 1-chloropropan-2-ol (bottom) for the two naturally abundant chlorine isotopes. All other isotopes are in their most naturally abundant form. Additional lines were measured for 2-gG', 2-g'G and 1-g'G in comparison to the study of Goldstein *et al.*^[6]. The Watson *S* Hamiltonian was used for all fits, including those that were taken from the Goldstein work. Furthermore, the root mean squared deviation between the fit and experiment σ_{RMS} and the number of assigned lines N_L are given as well as the maximum value of the (pseudo)-quantum numbers J^m , K_a^m , K_c^m and F^m involved in the assigned transitions and Ray's asymmetry parameter κ ^[14]. Moreover, it is noted whether or not transitions according to μ_a , μ_b or μ_c dipole components were observed. All values are given in MHz when applicable. Values in brackets for χ_{ij} were computed at the CCSD(T)-DKH2/awCVTZ level of theory and were fixed during the fit. In the nomenclature of Goldstein *et al.*^[6], g-ga, g'-gg, m-ga and h-gg correspond to 2-gG', 2-g'G, 1-gG' and 1-g'G, respectively.

	2-gG'		2-g'G	
	^{35}Cl	^{37}Cl	^{35}Cl	^{37}Cl
<i>A</i>	4670.461 28(16)	4588.024 23(28)	4938.132 13(21)	-
<i>B</i>	3309.859 34(18)	3270.719 28(27)	3130.873 60(23)	-
<i>C</i>	2076.153 44(15)	2044.539 02(13)	2352.391 41(27)	-
D_J	0.001 045 5(81)	0.001 128 6(74)	0.001 555 9(76)	-
D_K	0.001 543(11)	0.002 063(42)	0.006 071(28)	-
D_{JK}	-0.000 090 2(74)	-0.000 812(38)	-0.003 032(28)	-
d_1	-0.000 483 4(12)	-0.000 500 0(62)	-0.000 492 7(86)	-
d_2	-0.000 094 8(71)	-0.000 086 0(53)	-0.000 031 5(31)	-
χ_{aa}	13.6517(14)	8.1759(13)	-20.2271(14)	-
χ_{bb-cc}	-69.5087(26)	-52.3088(24)	-23.9061(24)	-
χ_{ab}	37.11(21)	30.94(19)	-41.76(65)	-
χ_{ac}	[-10.492]	[-8.988]	26.7(1.4)	-
χ_{bc}	22.57(31)	16.60(35)	21.46(65)	-
C_{aa}	-	-	-	-
C_{bb}	-	-	-	-
C_{cc}	-	-	-	-
μ_a	yes	yes	no	-
μ_b	yes	yes	yes	-

μ_c	no	no	yes	-
σ_{RMS}	0.0020	0.0015	0.0013	-
N_L	144	95	71	-
$J^{\text{m}}/K_a^{\text{m}}/K_c^{\text{m}}/F^{\text{m}}$	6/4/5/7.5	4/3/4/5.5	4/4/3/5.5	-
κ	-0.05	-0.04	-0.40	-
	^{35}Cl	1-gG'	^{35}Cl	1-g'G
		^{37}Cl		^{37}Cl
A	8474.336 91(39)	8473.426 98(95)	6086.0836(12)	6076.604 99(67)
B	2199.990 02(11)	2143.408 08(16)	2576.669 72(91)	2514.681 39(25)
C	1857.045 35(12)	1816.604 33(18)	2321.611 90(43)	2272.444 50(24)
D_J	0.000 323 3(32)	0.000 316 3(29)	0.000 794(25)	0.000 896(10)
D_K	0.004 223 0(32)	0.005 440(37)	-0.005 10(33)	-0.004 32(15)
D_{JK}	0.003 435 0(18)	0.003 35(15)	0.005 09(14)	0.004 410(54)
d_1	-0.000 055 8(10)	-0.000 049 40(67)	-0.000 127(21)	-
d_2	-0.000 013 5(14)	-	-0.000 012 2(35)	-0.000 057 8(87)
χ_{aa}	-45.0012(13)	-35.4877(19)	-17.2631(38)	-14.0686(17)
χ_{bb-cc}	-17.6403(28)	-13.9452(38)	55.5924(64)	43.3626(34)
χ_{ab}	-39.04(22)	-31.62(30)	[1.695] [1.329]	
χ_{ac}	20.21(48)	15.40(72)	-52.27(81)	-41.04(51)
χ_{bc}	10.28(27)	8.61(43)	[-0.023] [-0.027]	
C_{aa}	-	-	-	-
C_{bb}	-	-	-	-
C_{cc}	-	-	-	-
μ_a	yes	yes	yes	yes
μ_b	yes	yes	yes	yes
μ_c	yes	yes	yes	yes
σ_{RMS}	0.0018	0.0021	0.0031	0.0036
N_L	150	106	64	72
$J^{\text{m}}/K_a^{\text{m}}/K_c^{\text{m}}/F^{\text{m}}$	6/4/6/7.5	6/2/6/7.5	4/2/4/5.5	4/2/4/5.5
κ	-0.90	-0.90	-0.86	-0.87

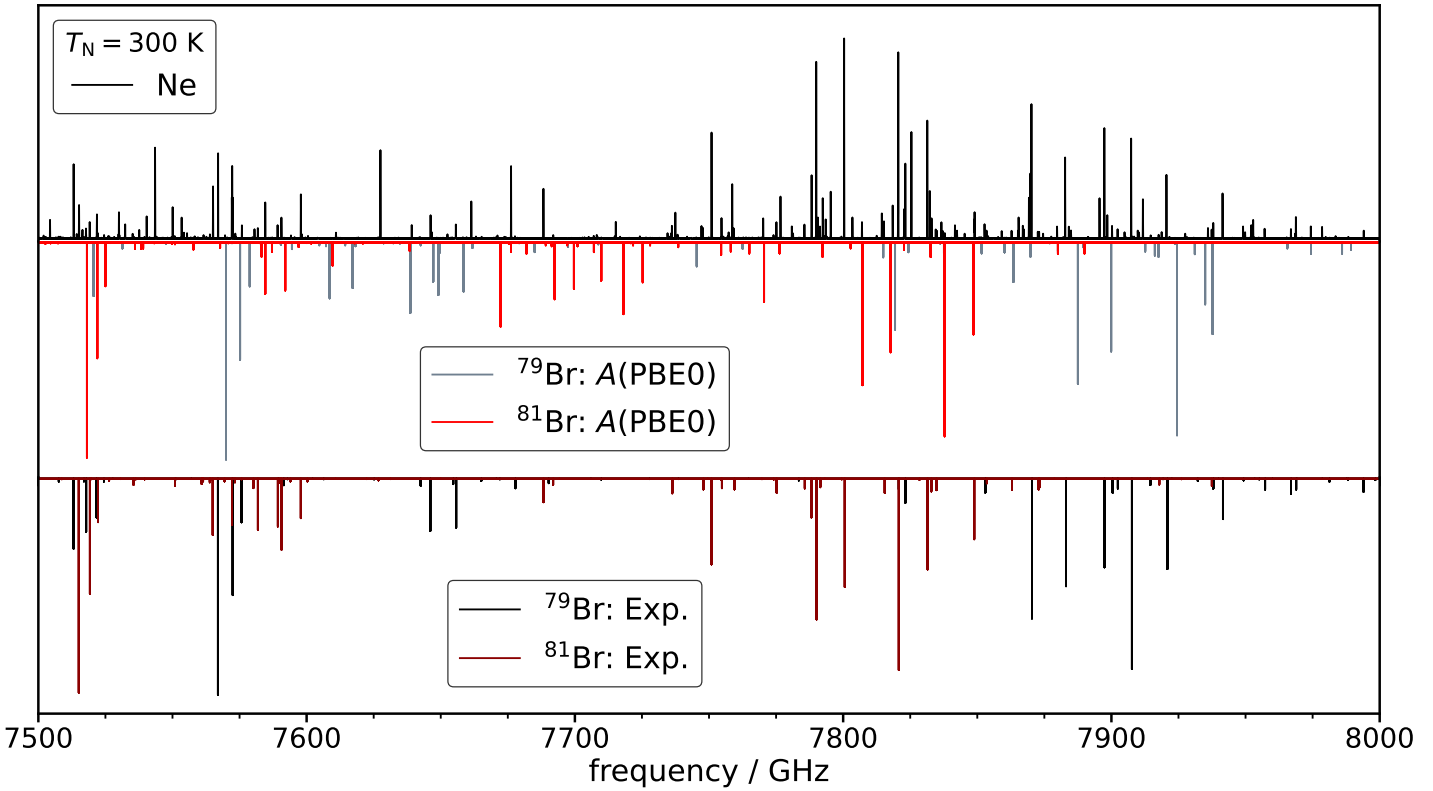


Fig. S4: Illustration of the impact of a change of the A rotational constant with 2-bromopropan-1-ol as an example. The top panel shows the experimental microwave spectrum, the middle panel an experimental fit with the A_e at the PBE0-D3(BJ)/aVTZ level of theory (^{79}Br : 3974.93 MHz and ^{81}Br : 3971.47 MHz) and the bottom panel a complete experimental fit (see Tab. S9). Only the simulations for 2-gG' are shown. It can immediately be seen that some parts of the fit are significantly impacted. For instances, substantial changes can be observed around 7800 MHz and 7900 MHz for ^{81}Br and ^{79}Br , respectively. This includes the spectral pattern but also the intensities of the transitions. However, for some bands, e.g. 7575 MHz, the impact is minor. This goes to show, that despite the fit describing some transition fairly well it can still be considerably off for others. For a purely theoretical prediction error compensation may keep correct patterns.

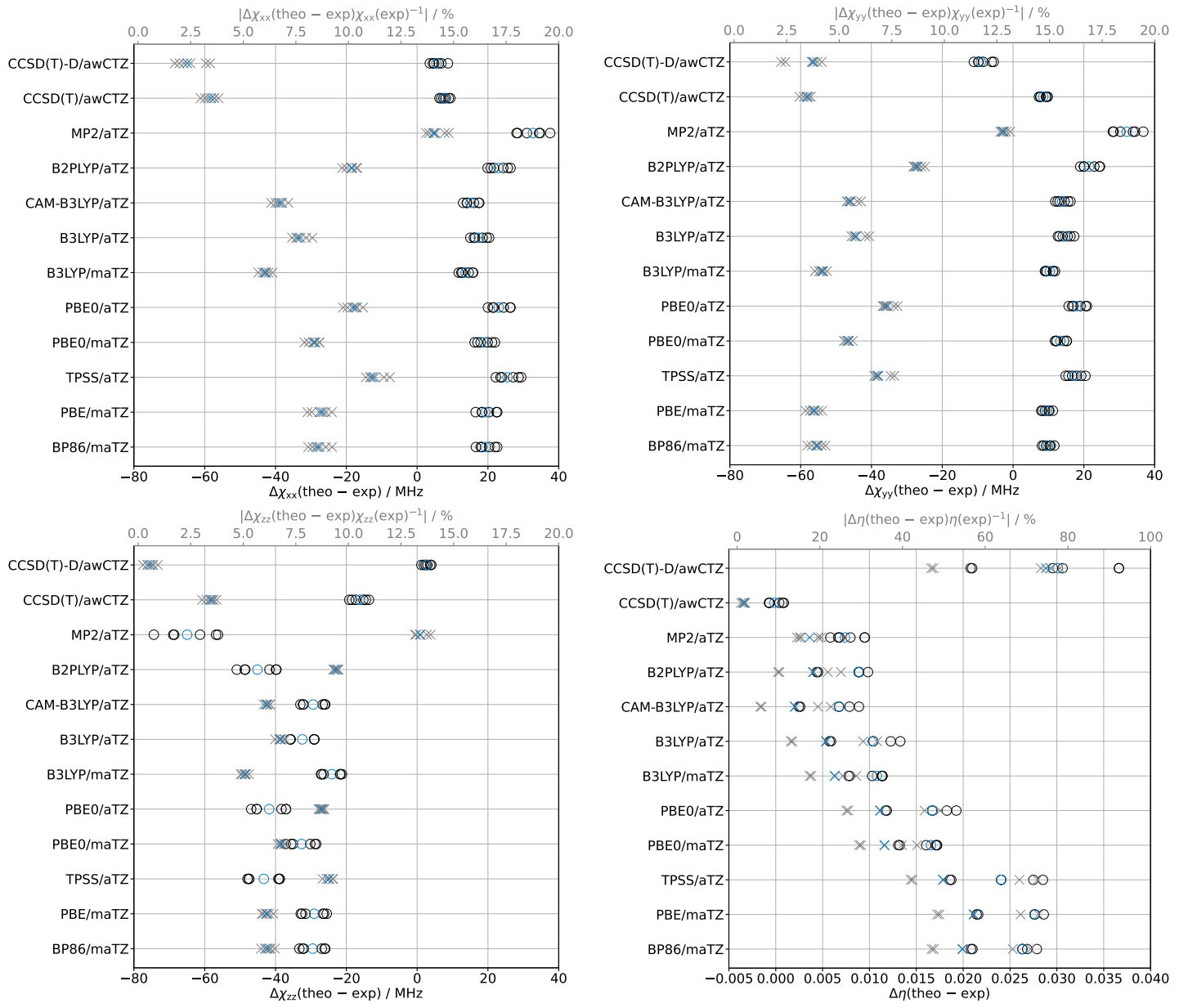


Fig. S5: Overview of the difference between the predicted and experimental values for the nuclear quadrupole coupling constants (in the axis system of the nucleus) χ_{xx} , χ_{yy} , χ_{zz} and η for the bromopropanols. The 1-g'G conformer is excluded from this analysis since the full χ tensor could not be experimentally determined. -D indicates the use of DKH2. In all cases, six datapoints are used. Additionally, absolute relative deviations are shown with grey crosses using the grey x -axis at the top. The corresponding median values are shown in blue. CCSD(T)/awCTZ performs exceptionally well to predict η . However, as the comparison of the individual χ components (χ_{xx} , χ_{yy} and χ_{zz}) shows it does not necessarily yield the best description in this case. Despite the fact that CCSDT-D/awCTZ overall performs better than the non-relativistic variant when predicting χ , it yields poor results for η . This indicates that CCSD(T)/awCTZ strongly profits from error compensation when predicting η . Hence, the use of η instead of individual χ components may be favourable since excellent results can be achieved with CCSD(T)/awCTZ. This is also reflected in the relative absolute deviation which do not exceed 2%. Absolute values for coupled cluster can be found in Tab. S11. Results using a pseudo-potential for the bromine atom at the CCSD(T) level are not shown here since the χ values deviate to such an extent from experiment that it would make the visualisation of the results extremely difficult. This highlights the importance of the core electrons for the electric field gradient and by extension χ .

Tab. S11: Overview of different values for the asymmetry parameter η for *trans*-1-X-propane, *gauche*-X-propane, 1-X-propanol (1-g'G' and 1-g'G), 2-X-propane and 2-X-propanol (2-g'G' and 2-g'G) with X being ^{35}Cl , ^{37}Cl , ^{79}Br and ^{81}Br . The underlying structures for the calculation of the electric field gradient were computed at the CCSD(T)-F12a/VDZ-F12 level. A comparison to experimental results for the bromopropanols can be found in Fig. S5. In case of bromine, calculations using a pseudo-potential (PP) for the Br atom were conducted. DKH2 indicates the use of the relativistic Douglas-Kroll-Hess correction of second order.

		^{35}Cl	^{37}Cl	^{79}Br	^{81}Br
<i>t</i> -1-X-propane	CCSD(T)/aug-cc-pwCVTZ	0.009 03	0.009 04	0.004 65	0.004 64
	CCSD(T)/aug-cc-pwCVTZ-PP	-	-	0.006 15	0.006 26
	CCSD(T)-DKH2/aug-cc-pwCVTZ	0.009 25	0.009 22	0.024 23	0.024 21
<i>g</i> -1-X-propane	CCSD(T)/aug-cc-pwCVTZ	0.018 92	0.018 92	0.016 69	0.016 70
	CCSD(T)/aug-cc-pwCVTZ-PP	-	-	0.018 31	0.018 24
	CCSD(T)-DKH2/aug-cc-pwCVTZ	0.019 05	0.019 033	0.036 83	0.036 84
1-g'G'	CCSD(T)/aug-cc-pwCVTZ	0.049 14	0.049 15	0.047 58	0.047 58
	CCSD(T)/aug-cc-pwCVTZ-PP	-	-	0.039 75	0.039 74
	CCSD(T)-DKH2/aug-cc-pwCVTZ	0.049 58	0.049 56	0.084 91	0.084 92
1-g'G	CCSD(T)/aug-cc-pwCVTZ	0.058 79	0.058 50	0.059 38	0.059 39
	CCSD(T)/aug-cc-pwCVTZ-PP	-	-	0.052 06	0.052 05
	CCSD(T)-DKH2/aug-cc-pwCVTZ	0.059 03	0.058 77	0.087 60	0.087 60
2-X-propane	CCSD(T)/aug-cc-pwCVTZ	0.014 96	0.014 95	0.015 45	0.015 44
	CCSD(T)/aug-cc-pwCVTZ-PP	-	-	0.015 46	0.015 45
	CCSD(T)-DKH2/aug-cc-pwCVTZ	0.014 81	0.014 79	0.003 37	0.003 37
2-g'G'	CCSD(T)/aug-cc-pwCVTZ	0.039 11	0.039 12	0.039 62	0.039 61
	CCSD(T)/aug-cc-pwCVTZ-PP	-	-	0.030 78	0.030 82
	CCSD(T)-DKH2/aug-cc-pwCVTZ	0.039 44	0.039 47	0.069 87	0.069 87
2-g'G	CCSD(T)/aug-cc-pwCVTZ	0.042 25	0.042 20	0.045 03	0.045 03
	CCSD(T)/aug-cc-pwCVTZ-PP	-	-	0.034 33	0.034 45
	CCSD(T)-DKH2/aug-cc-pwCVTZ	0.042 37	0.042 37	0.065 12	0.065 10

5 Conversion of τ to the quartic centrifugal distortion constants

Equations 1 to 5 show the relationship of $\tau'_{\alpha\alpha\beta\beta}$ ($\alpha, \beta = (x, y, z), (x, y, z)$), the non-reduced quartic centrifugal distortion constants (CDC) in MHz, to the quartic centrifugal distortion constants within the Watson *A* reduction, while 6 to 10 show the connection between the Watson *A* and *S* reduction. In this work, the I^r representation has been used so that $z \mapsto a$, $x \mapsto b$ and $y \mapsto c$ and the *S* reduction was employed. $\tau'_{\alpha\alpha\beta\beta}$ is directly computed by Gaussian and can be used to ensure the correct reduction and representation is compared to the experiment. The formulas are taken from Ref. [15] and a derivation can be found therein. It is important to point out, that the distortion constants computed with VPT2 in this manner are equilibrium values as is also indicated by the use of equilibrium rotational constants B_e^α . Furthermore, $\tau'_{\alpha\alpha\beta\beta}$ is derived from harmonic frequency calculations. Vibrational corrections are first included at fourth-order, *i.e.* VPT4.

$$\Delta_J = -\frac{1}{8} (\tau'_{xxxx} + \tau'_{yyyy}) \quad (1)$$

$$\Delta_K = -\frac{1}{4} (\tau'_{xxxx} + \tau'_{yyyy} + \tau'_{zzzz}) + \frac{1}{4} (\tau'_{yyzz} + \tau'_{xxzz} + \tau'_{xxyy}) \quad (2)$$

$$\Delta_{JK} = \frac{3}{8} (\tau'_{xxxx} + \tau'_{yyyy}) - \frac{1}{4} (\tau'_{yyzz} + \tau'_{xxzz} + \tau'_{xxyy}) \quad (3)$$

$$\delta_J = -\frac{1}{16} (\tau'_{xxxx} - \tau'_{yyyy}) \quad (4)$$

$$\delta_K = \frac{1}{8} \left[\tau'_{xxxx} \left(\frac{B_e^x - B_e^z}{B_e^x - B_e^y} \right) + \tau'_{yyyy} \left(\frac{B_e^y - B_e^z}{B_e^x - B_e^y} \right) + \tau'_{yyzz} - \tau'_{xxzz} + \tau'_{xyzy} \sigma \right] \quad (5)$$

$$D_J = \Delta_J + 2d_2 = \Delta_J - \frac{\delta_K}{2\sigma} \quad (6)$$

$$D_K = \Delta_K + 10d_2 = \Delta_K - \frac{5\delta_K}{2\sigma} \quad (7)$$

$$D_{JK} = \Delta_{JK} - 12d_2 = \Delta_{JK} + \frac{3\delta_K}{\sigma} \quad (8)$$

$$d_1 = -\delta_J \quad (9)$$

$$d_2 = -\frac{\delta_K}{4\sigma} \quad (10)$$

$$\sigma = \frac{2B_e^z - B_e^x - B_e^y}{B_e^x - B_e^y} \quad (11)$$

At the coupled cluster level, the CDCs were calculated following Watson^[16] via

$$\tau'_{\alpha,\alpha,\beta,\beta} = -2 \sum_k \frac{(\tilde{B}_e^\alpha)^2 (\tilde{B}_e^\beta)^2}{\omega_k} \cdot \left[\varepsilon_k^{\alpha,\alpha} \varepsilon_k^{\beta,\beta} + 2(\varepsilon_k^{\alpha,\beta})^2 \cdot (1 - \delta_{\alpha,\beta}) \right], \quad (12)$$

where ω_k is the harmonic wavenumber of the k th vibration, $\tilde{B}_e^\alpha = (B_e^\alpha/c)$ is the equilibrium rotational constant about axis α in wavenumbers, and $\varepsilon_k^{\alpha,\beta}$ is proportional to the first derivative of the equilibrium inertia tensor with respect to dimensionless normal coordinates (q_k). All three parameters are expressed in wavenumbers or wavelengths. Following the definition of Gong *et al.* to include the factor $(2hc/\hbar^2)$,^[17] $\varepsilon_k^{\alpha,\beta}$ (reserving $a_k^{\alpha,\beta}$ for $\partial I^{\alpha,\beta}/\partial Q_k|_e$) is given by

$$\varepsilon_k^{\alpha,\beta} = \frac{2hc}{\hbar^2} \frac{\partial I^{\alpha,\beta}}{\partial q_k} \Big|_e \quad (13)$$

and is related to $B_k^{\alpha,\beta}$ by Aliev and Mikhaylov and the dimensionless $C_k^{\alpha,\beta}$ by Watson (see Ref. [16, Sec. IV.A]) via

$$\varepsilon_k^{\alpha,\beta} = -\frac{B_k^{\alpha,\beta}}{\tilde{B}_e^\alpha \tilde{B}_e^\beta} = \frac{\omega_k C_k^{\alpha,\beta}}{\tilde{B}_e^\alpha \tilde{B}_e^\beta}. \quad (14)$$

6 Additional vibrational analysis

In Fig. S6 the experimental and predicted hydrogen bond shifts between the gG' and g'G conformers ($\Delta\tilde{\nu}$) are compared for the chloro- and bromopropanols, which include MP2/6-311++G(d,p) values that have been computed by Goldstein *et al.*[6]. For a detailed discussion of the bromopropanols see the main text. The results of the chloropropanols are remarkably similar to the bromopropanols, and all trends observed for one can be transferred to the other. Firstly, the harmonic hydrogen bond shifts (\times) are discussed. The GGA functionals BP86 and PBE perform the worst consistently yielding values that are too small. The meta-GGA TPSS slightly remedies this problem. The hybrid functionals PBE0 and B3LYP perform better but still yield shifts that are too small. The range-separated hybrid CAM-B3LYP functional performs the best of all functionals and even outperform the double hybrid functional B2PLYP, which more closely resembles the results of B3LYP and PBE0. MP2/aTZ yields good predictions for 2-chloropropan-1-ol (red) but severely underestimates the shift for 1-chloropropan-2-ol (black). The additional 6-311++G(d,p) basis sets exacerbates this behaviour. The coupled cluster results are quite close to the experimental values.

Anharmonic corrections (+) are mostly counter-productive for 2-chloropropan-1-ol, whereas for 1-chloropropan-2-ol they point in the right direction. Especially, CAM-B3LYP yields an excellent prediction for 1-chloropropan-2-ol. The strength of the anharmonic correction is also more significant for 1-chloropropan-2-ol. Furthermore, transferring the anharmonic trends to the CCSD(T) results leads to almost perfect predictions.

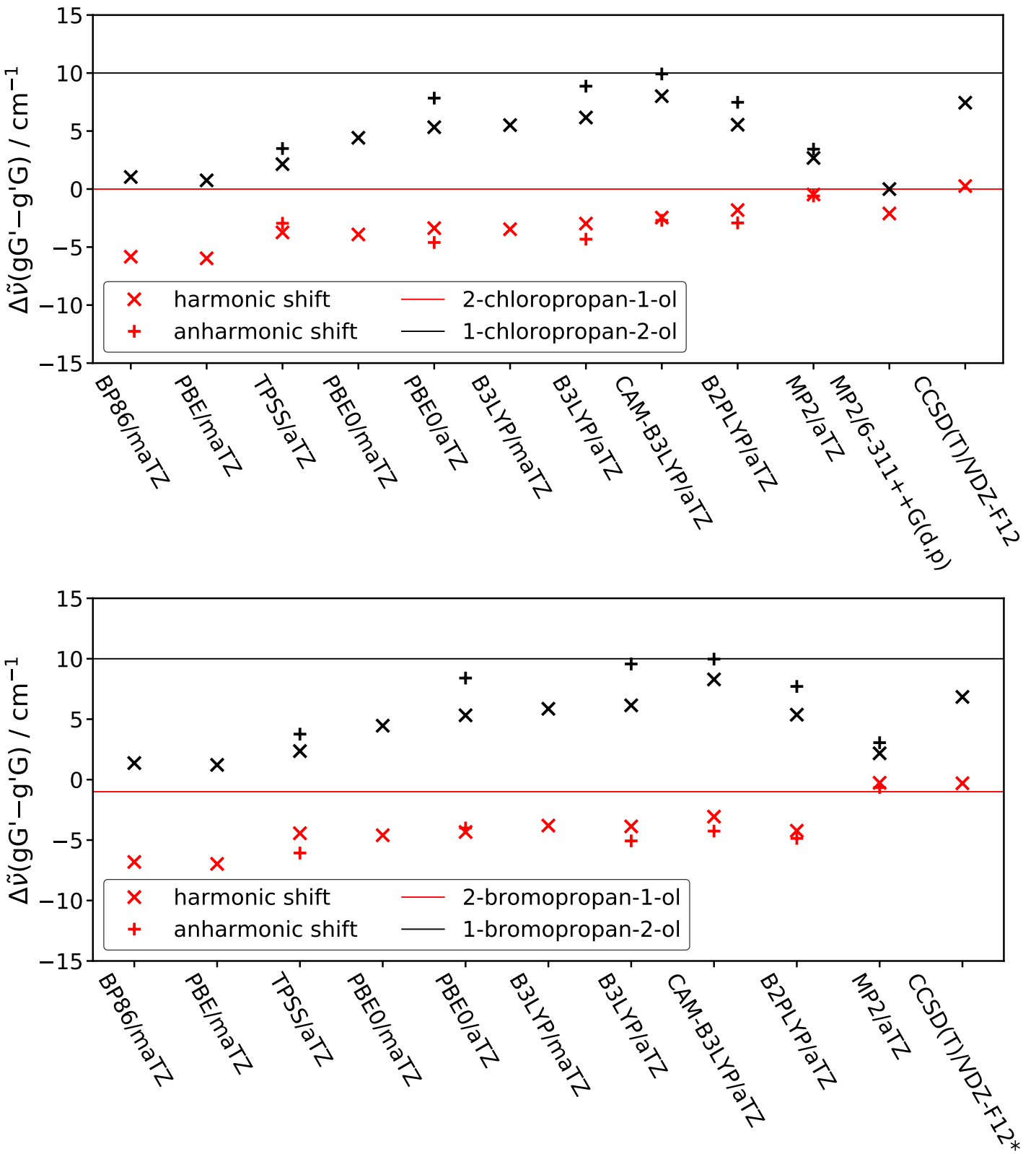


Fig. S6: Overview of the predicted harmonic (\times) and anharmonic (+) hydrogen bond shifts. The results for the chloropropanols are shown in the top and the ones for bromopropanols in the bottom panel. The experimental values are indicated by the red and black line for 2-chloro/bromopropan-1-ol and 1-chloro/bromopropan-2-ol, respectively. The MP2/6-311++G(d,p) values were taken from Ref. [6].

The absolute band predictions of the chloro- and bromopropanols are compared in Tab. S12. In general, the behaviour between the chloro- and bromopropanols is quite similar. Here, a detailed analysis of the chloro-

propanols will be given. A detailed discussion of the bromopropanols is given in the main text. As was the case for the bromopropanols, the harmonic predictions of the GGAs are very inconsistent as indicated by the standard deviation. However, BP86 remains fairly close to the experiment. The meta-GGA TPSS performs slightly better in terms of consistency but still significantly deviates from the experiment. Directly comparing the different halogens shows no consistency between Br and Cl. Hence, no meaningful empirical correction can be made. The anharmonic TPSS values again strongly underestimate the OH stretching frequencies. However, in comparison to the bromopropanols, σ is significantly smaller, *i.e.*, by 0.7 cm^{-1} . PBE0 shows a slightly smaller spread (smaller σ) with the mean again being different from that found for the bromopropanols, although in either case the OH stretching frequencies are overestimated. B3LYP, CAM-B3LYP and B2PLYP behave very similar in terms of σ and the mean in comparison to the bromopropanols. This is especially true for the latter method, where the mean differs by only 1 cm^{-1} and σ by 0.1 cm^{-1} . Hence, B2PLYP can indeed again be empirically corrected by about $+13\text{ cm}^{-1}$ to yield good predictive capabilities. The results of a correction by the mean of the bromopropanols is shown in Tab. S13, further illustrating the advantages of an empiric correction of B2PLYP. This correction can even be extended to more complex 3-chloro- and 3-bromopropane-1,2-diols. To a lesser extent, CAM-B3LYP followed by B3LYP. For MP2, the results differ significantly from those found for the bromopropanols although σ remains fairly consistent.

Tab. S12: Overview of the difference between the predicted and calculated OH stretching frequencies of different computational methods for the chloropropanols (top) and bromopropanols (bottom). The first three methods (BP86, PBE and TPSS) are harmonic values. All other deviations shown are anharmonic deviations. For each method, the mean value as well as the standard deviation (σ) are shown. 1-Cl-gG' and 1-Cl-g'G refer to 1-chloropropan-2-ol, while 2-Cl-gG' and 2-Cl-g'G refer to 2-chloropropan-1-ol. For the bromine analogues, Cl is replaced by Br in its name. Positive values indicate overestimation and negative signs underestimation by a given method. All values are given in cm^{-1} .

	harmonic			anharmonic					
	BP86	PBE	TPSS	TPSS	PBE0	B3LYP	CAM-B3LYP	B2PLYP	MP2
1-Cl-gG'	1.1	12.4	29.7	-164.6	15.9	-32.2	22.9	-13.8	-9.0
1-Cl-g'G	6.9	18.3	33.5	-161.6	20.5	-27.9	25.6	-10.9	-8.4
2-Cl-gG'	13.1	24.0	37.8	-155.0	24.7	-24.7	28.6	-10.2	-9.4
2-Cl-g'G	4.2	14.8	30.0	-161.5	22.5	-25.9	28.5	-12.7	-16.0
mean	6.3	17.4	32.8	-160.7	20.9	-27.7	26.4	-11.9	-10.7
σ	5.1	5.1	3.8	4.0	3.8	3.3	2.7	1.7	3.5
1-Br-gG'	-6.0	4.7	22.5	-176.5	11.0	-33.7	25.7	-14.9	-16.3
1-Br-g'G	-0.2	10.7	25.9	-171.4	14.0	-29.6	29.0	-11.0	-16.7
2-Br-gG'	6.7	16.7	30.7	-165.0	18.8	-26.4	31.1	-12.0	-17.2
2-Br-g'G	-2.0	7.9	23.0	-171.3	17.2	-26.9	31.1	-14.3	-24.1
mean	-0.4	10.0	25.5	-171.0	15.3	-29.2	29.2	-13.1	-18.6
σ	5.3	5.1	3.8	4.7	3.5	3.3	2.5	1.8	3.7

Tab. S13: Deviations from experiment for the chloropropanols corrected by the mean of the bromopropanols shown in Tab. S12. The first three methods (BP86, PBE and TPSS) are harmonic values. All other deviations shown are anharmonic deviations. For each method, the absolute mean value is shown. 1-Cl-gG' and 1-Cl-g'G refer to 1-chloropropan-2-ol while 2-Cl-gG' and 2-Cl-g'G refer to 2-chloropropan-1-ol. Positive values indicate overestimation and negative signs underestimation by a given method. All values are given in cm^{-1} .

	harmonic			anharmonic					
	BP86	PBE	TPSS	TPSS	PBE0	B3LYP	CAM-B3LYP	B2PLYP	MP2
1-Cl-gG'	1.4	2.4	4.2	6.4	0.6	-3.0	-6.3	-0.7	9.6
1-Cl-g'G	7.3	8.3	7.9	9.4	5.2	1.3	-3.6	2.2	10.2
2-Cl-gG'	13.5	14.0	12.3	16.0	9.4	4.5	-0.6	2.9	9.2
2-Cl-g'G	4.6	4.7	4.5	9.5	7.2	3.3	-0.7	0.4	2.6
abs. mean	6.7	7.3	7.2	10.3	5.6	3.0	2.8	1.6	7.9

7 Example inputs

7.1 ORCA

Tab. S14: Example inputs for the ORCA 4.2.1^[18–20] calculations. Numerical frequency calculations are needed to compute the Raman activities. For BP86 and PBE the RI-J approximation was used. The %eprnmr block follows after the geometry input. Only the method block is shown.

calculation	input
optimisation + analytical frequencies	<pre> !B3LYP D3BJ abc UseSym ma-def2-TZVP TightOpt TightSCF Freq Grid5 NoFinalGrid Mass2016 %method SymThresh 5.0e-2 end </pre>
optimisation + numerical frequencies	<pre> !B3LYP D3BJ abc UseSym RIJCOSX def2/J ma-def2-TZVP TightOpt TightSCF NumFreq Grid5 NoFinalGrid GridX4 Mass2016 %method SymThresh 5.0e-2 end %elprop Polar 1 end </pre>
electric field gradient	<pre> !CCSD(T) aug-cc-pwCVTZ NoFrozenCore NoRI TightSCF Grid7 Mass2016 %eprnmr nuclei = all Br {fgrad} end </pre>
electric field gradient + DKH2	<pre> !CCSD(T) DKH2 aug-cc-pwCVTZ NoFrozenCore NoRI TightSCF Grid7 Mass2016 %rel FiniteNuc true picturechange 2 end %eprnmr nuclei = all Br {fgrad} end </pre>

7.2 Gaussian

Tab. S15: Example inputs for the Gaussian 16 (Rev. A.03)^[21] calculations at the B3LYP level of computation. The Print and Resonances settings follow one line after the geometry input. Only the method block is shown.

calculation	input
optimisation DFT + VPT2	# B3LYP aug-cc-pVTZ Int=SuperFine output=pickett # Opt=VeryTight empiricaldispersion=gd3bj # Freq=(anharmonic,ReadAnharm) Print=(NMOrder=AscNoIrrep) Resonances=No11Res
optimisation WFT + VPT2	# MP2 aug-cc-pVTZ output=pickett # Opt=VeryTight # Freq=(anharmonic,ReadAnharm) Print=(NMOrder=AscNoIrrep) Resonances=No11Res

7.3 Molpro

Tab. S16: Example input for the MOLPRO 2020.2^[22–24] calculations at CCSD(T) level with specialised option for the use of the VDZ-PP-F12 basis set. For CI the definitions simplify to basis=vdz-f12 with all other auxiliary basis set definitions becoming obsolete. Only the method block is shown.

```
basis={default=vdz-f12;
br=VDZ-PP-F12
set,df
default=AUG-CC-PVDZ/mp2fit;
br=VDZ-PP-F12/mp2fit
set,jk
default=AUG-CC-PVDZ/jkfit;
br=def2-QZVPP/jkfit
set,ri
default=vdz-f12/optri;
br=VDZ-PP-F12/optri}
gthresh,OPTSTEP=6.d-5,OPTGRAD=1.d-6,ENERGY=1.d-10,ZERO=1.d-16
orient,NOORIENT
symmetry
MASS,ISO
geomtyp=xyz
angstrom
geometry=GEOM_START.xyz
explicit,ri_basis=ri,df_basis=dfmp,df_basis_exch=jk
{hf,accu,16}
{df-ccsd(t)-f12a,ansatz=3*C(FIX,HY1),cabs=0,cabs_singles=0,
ri_basis=ri,df_basis=df,df_basis_exch=jk}
{OPTG,GAUSSIAN,GRMS=1.d-5,SRMS=1.d-5}
put,xyz,GEOM.xyz
{frequencies
PRINT,HESSIAN,LOW}
```

Literature

- [1] B. Hartwig, "Diols under Investigation: Benchmarking their Monomers, Dimers and Chirality Recognition", PhD thesis, Georg-August-Universität Göttingen, Germany, **2022**.
- [2] U. Andresen, H. Dreizler, U. Kretschmer, W. Stahl, C. Thomsen, "A molecular beam Fourier transform microwave spectrometer developed for analytical purposes", *Fresenius' journal of analytical chemistry* **1994**, *349*, 272–276.
- [3] M. Schnell, D. Banser, J. U. Grabow, "Coaxially aligned electrodes for Stark-effect applied in resonators using a supersonic jet Fourier transform microwave spectrometer", *Review of Scientific Instruments* **2004**, *75*, 2111–2115.
- [4] B. Hartwig, "Monomer Raman-Spectra of Mono- and Diols in the 3700 to 3560 Wavenumber Range", *Göttingen Research Online / Data* **2022**, version V1, DOI: 10.25625/EJVBHD.
- [5] K. M. S. Gonçalves, D. R. Garcia, T. C. Ramalho, J. D. Figueroa-Villar, M. P. Freitas, "Conformational Analysis of 1-Chloro- and 1-Bromo-2-propanol", *J. Phys. Chem. A* **2013**, *117*, 10980–10984.
- [6] T. Goldstein, M. Snow, B. Howard, "Intramolecular hydrogen bonding in chiral alcohols: The microwave spectrum of the chloropropanols", *J. Mol. Spectrosc.* **2006**, *236*, 1–10.
- [7] S. Grimme, "Supramolecular Binding Thermodynamics by Dispersion-Corrected Density Functional Theory", *Chem. Eur. J.* **2012**, *18*, 9955–9964.
- [8] K. E. Otto, Z. Xue, P. Zielke, M. A. Suhm, "The Raman spectrum of isolated water clusters", *Phys. Chem. Chem. Phys.* **2014**, *16*, 9849–9858.
- [9] T. N. Wassermann, M. A. Suhm, "Ethanol Monomers and Dimers Revisited: A Raman Study of Conformational Preferences and Argon Nanocoating Effects", *J. Phys. Chem. A* **2010**, *114*, 8223–8233.
- [10] T. N. Wassermann, M. A. Suhm, P. Roubin, S. Coussan, "Isomerization around C–C and C–O bonds in 1-propanol: Collisional relaxation in supersonic jets and selective IR photo-isomerization in cryogenic matrices", *J. Mol. Struct.* **2012**, *1025*, Light-Induced Processes in Cryogenic Matrices, 20–32.
- [11] H. Schaal, T. Häber, M. A. Suhm, "Hydrogen Bonding in 2-Propanol. The Effect of Fluorination", *J. Phys. Chem. A* **2000**, *104*, 265–274.
- [12] T. Schrage, T. N. Wassermann, M. A. Suhm, *Z. Phys. Chem.* **2008**, *222*, 1407–1452.
- [13] J. Durig, S. Shen, G. Guirgis, "Far infrared spectra, conformational equilibria, vibrational assignments, ab initio calculations and structural parameters for 2-bromoethanol", *J. Mol. Struct.* **2001**, *560*, 295–314.
- [14] B. S. Ray, "Über die Eigenwerte des asymmetrischen Kreisels", *Z. Phys.* **1932**, *78*, 74–91.
- [15] W. Gordy, R. Cook, *Microwave Molecular Spectra*, Interscience Pub., **1970**.
- [16] J. K. G. Watson in *Vibrational spectra and structure*, Vol. 6, (Ed.: J. R. Durig), Elsevier Scientific Publishing Company, Amsterdam, **1977**, pp. 1–89.
- [17] J. Z. Gong, D. A. Matthews, P. B. Changala, J. F. Stanton, "Fourth-order vibrational perturbation theory with the Watson Hamiltonian: Report of working equations and preliminary results", *J. Chem. Phys.* **2018**, *149*, 114102.
- [18] F. Neese, "The ORCA Program System", *WIREs Comput. Mol. Sci.* **2012**, *2*, 73–78.
- [19] F. Neese, "Software Update: The ORCA Program System, Version 4.0", *WIREs Comput. Mol. Sci.* **2017**, *8*, e1327.
- [20] F. Neese, F. Wennmohs, U. Becker, C. Ripplinger, "The ORCA quantum chemistry program package", *J. Chem. Phys.* **2020**, *152*, 224108.

- [21] M. J. Frisch, G. W. Trucks, H. B. Schlegel, G. E. Scuseria, M. A. Robb, J. R. Cheeseman, G. Scalmani, V. Barone, G. A. Petersson, H. Nakatsuji, X. Li, M. Caricato, A. V. Marenich, J. Bloino, B. G. Janesko, R. Gomperts, B. Mennucci, H. P. Hratchian, J. V. Ortiz, A. F. Izmaylov, J. L. Sonnenberg, D. Williams-Young, F. Ding, F. Lipparini, F. Egidi, J. Goings, B. Peng, A. Petrone, T. Henderson, D. Ranasinghe, V. G. Zakrzewski, J. Gao, N. Rega, G. Zheng, W. Liang, M. Hada, M. Ehara, K. Toyota, R. Fukuda, J. Hasegawa, M. Ishida, T. Nakajima, Y. Honda, O. Kitao, H. Nakai, T. Vreven, K. Throssell, J. A. Montgomery, Jr., J. E. Peralta, F. Ogliaro, M. J. Bearpark, J. J. Heyd, E. N. Brothers, K. N. Kudin, V. N. Staroverov, T. A. Keith, R. Kobayashi, J. Normand, K. Raghavachari, A. P. Rendell, J. C. Burant, S. S. Iyengar, J. Tomasi, M. Cossi, J. M. Millam, M. Klene, C. Adamo, R. Cammi, J. W. Ochterski, R. L. Martin, K. Morokuma, O. Farkas, J. B. Foresman, D. J. Fox, Gaussian 16 Revision A.03, Gaussian Inc. Wallingford CT, **2016**.
- [22] H.-J. Werner, P. J. Knowles, G. Knizia, F. R. Manby, M. Schütz, “Molpro: a general-purpose quantum chemistry program package”, *WIREs Comput. Mol. Sci.* **2012**, *2*, 242–253.
- [23] H.-J. Werner, P. J. Knowles, F. R. Manby, J. A. Black, K. Doll, A. Heßelmann, D. Kats, A. Köhn, T. Korona, D. A. Kreplin, Q. Ma, T. F. Miller, A. Mitrushchenkov, K. A. Peterson, I. Polyak, G. Rauhut, M. Sibaev, “The Molpro quantum chemistry package”, *J. Chem. Phys.* **2020**, *152*, 144107.
- [24] H.-J. Werner, P. J. Knowles, G. Knizia, F. R. Manby, M. Schütz, P. Celani, W. Györffy, D. Kats, T. Korona, R. Lindh, A. Mitrushenkov, G. Rauhut, K. R. Shamasundar, T. B. Adler, R. D. Amos, S. J. Bennie, A. Bernhardsson, A. Berning, D. L. Cooper, M. J. O. Deegan, A. J. Dobbyn, F. Eckert, E. Goll, C. Hampel, A. Hesselmann, G. Hetzer, T. Hrenar, G. Jansen, C. Köpll, S. J. R. Lee, Y. Liu, A. W. Lloyd, Q. Ma, R. A. Mata, A. J. May, S. J. McNicholas, W. Meyer, T. F. M. III, M. E. Mura, A. Nicklass, D. P. O'Neill, P. Palmieri, D. Peng, T. Petrenko, K. Pfleiderer, R. Pitzer, M. Reiher, T. Shiozaki, H. Stoll, A. J. Stone, R. Tarroni, T. Thorsteinsson, M. Wang, M. Welborn, MOLPRO, version 2020.2, a package of ab initio programs, see <https://www.molpro.net>, **2020**.